Computational study of transport properties of graphene upon adsorption of an amino acid: importance of including – $\hbox{NH}_{2}$ NH 2 and –COOH groups

S. J. Rodríguez, L. Makinistian & E. Albanesi

⚫ Springer

Springer

CrossMark

Computational study of transport properties of graphene upon adsorption of an amino acid: importance of including –NH2 and –COOH groups

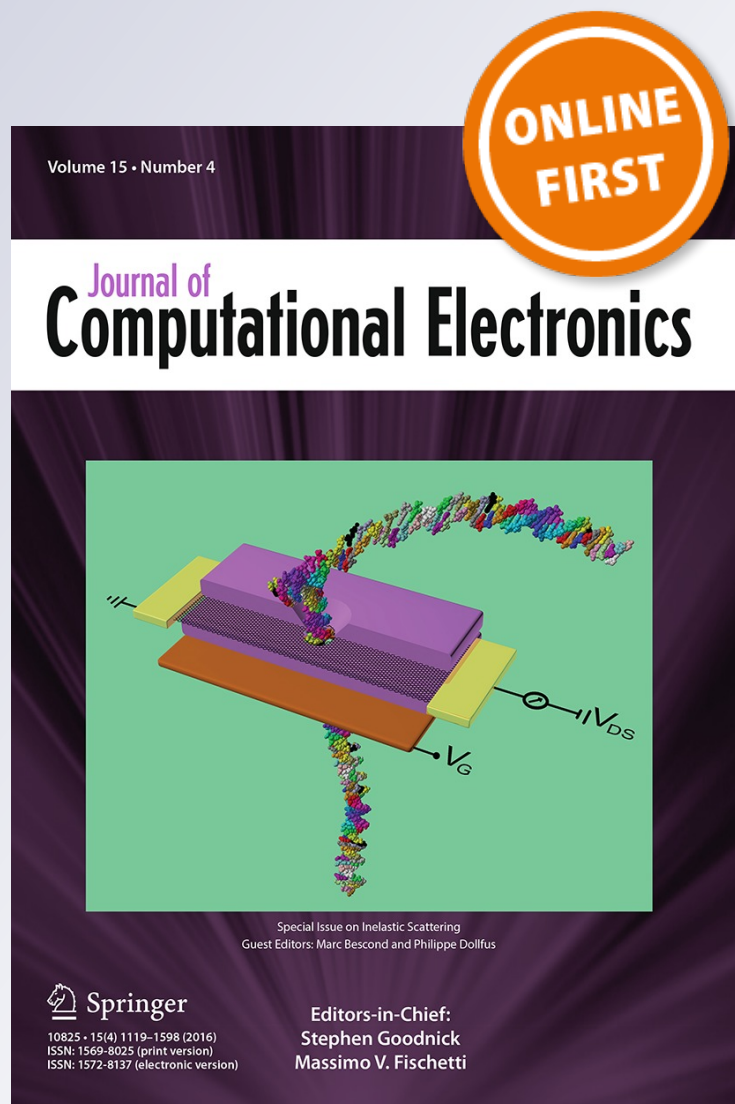S. J. Rodríguez[1,2] · L. Makinistian[3] · E. Albanesi[1,2]

Abstract The effects of histidine and its imidazole ring adsorption on the electronic transport properties of graphene were investigated by first-principles calculations within a combination of density functional theory and non-equilibrium Greens functions. Firstly, we report adsorption energies, adsorption distances, and equilibrium geometrical configurations with no bias voltage applied. Secondly, we model a device for the transport properties study: a central scattering region consisting of a finite graphene sheet with the adsorbed molecule sandwiched between semi-infinite source (left) and drain (right) graphene electrode regions. The electronic density, electrical current, and electronic transmission were calculated as a function of an applied bias voltage. Studying the adsorption of the two systems, i.e., the histidine and its imidazole ring, allowed us to evaluate the importance of including the carboxyl (–COOH) and amine (–NH2) groups. We found that the histidine and the imidazole ring affects differently the electronic transport through the graphene sheet, posing the possibility of graphene-based sensors with an interesting sensibility and specificity.

Keywords Adsorption amino acid · Graphene · NEGF

✉ S. J. Rodríguez
sindy.rodriguez@ifis.santafe-conicet.gov.ar

1   Instituto de Física del Litoral (CONICET-UNL), Güemes 3450, 3000 Santa Fe, Argentina

2   Facultad de Ingeniería, Universidad Nacional de Entre Ríos, 3101 Oro Verde, ER, Argentina

3   Departamento de Física, e Instituto de Física Aplicada (INFAP), Universidad Nacional de San Luis-CONICET, Ejército de los Andes 950, D5700BWS San Luis, Argentina

1 Introduction

Graphene is a semimetal with zero energy bandgap, and the carbon atoms are arranged in a hexagonal lattice in a single-atom-thick planar sheet. In comparison with other 3D materials, graphene has unique physical and chemical properties: high carrier mobility (can exceed $\approx 15,000 \, \text{cm}^2 \, \text{V}^{-1} \, \text{s}^{-1}$ even under ambient conditions), extremely high surface-to-volume ratio, flexibility, transparency, and biocompatibility, among others [1]. These features make it a good candidate for a new generation of electronic devices and bionic technology. In particular, the construction of nanobiosensors has become increasingly relevant because many biological processes and pharmacological responses may be monitored if biomolecules are detected and quantified [2]. Sensors for biological application must be biocompatible, sensitive, selective, and also with excellent electrical properties (such as a low intrinsic electronic noise): graphene could play an important role in this area. For instance, Baraket et al. [3] showed experimentally that aminated graphene can work as a biologically active field-effect transistor for DNA detection. Also, several theoretical and experimental studies have proposed the use of graphene in the construction of biosensors [2–7], e.g., graphene to detect glucose [8], proteins [9], DNA [10], or even bacteria [11,12].

Several biomolecules tend to bind to graphene through non-covalent bonds, such as $\pi-\pi$ stacking interaction. These interactions are relevant in the design and fabrication of nanodevices, because subtle changes in the electronic characteristics of the π systems with graphene can lead to relevant defects in the nanosystem structure and properties [5]. Theoretical studies based on ab initio calculations have been instrumental in understanding the nature of $\pi-\pi$ interactions. Song et al. [13] reported that oxygen in nucleobases adsorbed on graphene with $\pi-\pi$ stacking interaction alters the elec-

tric current in the graphene sheet. Lee [14] investigated the effects of DNA nucleotide adsorption on the conductance of graphene nanoribbons and found that, for the adsorption of a single nucleotide, the negatively charged phosphate produces conductance dips associated with quasi-bound states, reducing the hole conductance. Zhang et al. [15] studied the binding of organic donor, acceptor, and metal atoms on graphene sheets, revealing the effect of the different non-covalent functionalizations on the electronic structure and transport properties of graphene.

In this work, we present the results of modeling from first principles the adsorption of histidine on a graphene sheet. In order to discuss the importance of including the carboxyl (–COOH) and amine (–NH$_2$) groups in the adsorption on graphene, the calculations were performed for two systems: (1) histidine and (2) imidazole ring (i.e., histidine without the –COOH and –NH$_2$ groups). Additionally, we report the effects caused by the molecules adsorption on the electronic transport properties of graphene. The electronic transport has been explored in three different cases: (a) graphene sheet alone, (b) graphene with an adsorbed histidine, and (c) graphene with an adsorbed imidazole ring.

In a previous work [16], we studied the adsorption of histidine and imidazole ring on graphene using three approaches to the exchange and correlation interactions: local LDA, generalized gradients GGA-PBE, and van der Waals DFT-D2. The calculations demonstrated that adsorption energies satisfied the relation $E_{\text{ads-DFT-D2}} > E_{\text{ads-LDA}} > E_{\text{ads-GGA-PBE}}$; the adsorption distance for histidine met the relation $d_{\text{ads-DFT-D2}} < d_{\text{ads-LDA}} < d_{\text{ads-GGA-PBE}}$, while for the imidazole ring $d_{\text{ads-LDA}} < d_{\text{ads-DFT-D2}} < d_{\text{ads-GGA-PBE}}$. We also reported an underestimation of the adsorption energy and an overestimation of the adsorption distance in the GGA-PBE approach. We found a strong physisorption between histidine and graphene only when considering the van der Waals forces, which is in agreement with the literature [17,18]. We reported a charge transfer from the graphene sheet to the molecule higher for the DFT-D2 approach. The LDA and GGA-PBE approximation does not accurately represent the π–π bonds in the graphene molecule interface; consequently, the charge transfer is underestimated. Therefore, in this work we analyze the electronic transport only within the van der Waals DFT-D2 approach.

2 Computational details

Ab initio calculations were carried out using a pseudo-potential approach within DFT-D2 [19] as implemented in Openmx package. Numerical pseudo-atomic orbitals (PAOs) were used as the basis to expand one-particle Kohn–Sham wave functions [20]. The PAOs were specified by H5.0-$s1$, C5.0-$s2p2$, O6.0-$s2p2d1$, N6.0-$s2p2d1$, where H, C, O, and

N are the atomic symbols (i.e., hydrogen, carbon, oxygen, and nitrogen, respectively), 5.0 and 6.0 represent the cutoff radius (Bohr) in the generation by the confinement scheme, and for instance, "$s2p2d1$" indicates the employment of two primitive orbitals for each of the s and p components and one primitive orbital for the d component. First we studied the adsorption of the molecules on graphene (histidine and imidazole ring). Subsequently, we modeled a device to study the effects of the molecules on the electronic transport of graphene.

In order to obtain the interaction energy (E_{int}) and the adsorption distance (d_{ads}), the systems were modeled with an orthorhombic supercell of $12.78 \times 12.29 \times 25.00\,\text{Å}^3$ (these dimensions are sufficient to uncouple the graphene sheets and to avoid interactions between molecules of adjacent cells). All atoms were left to relax up to a convergence of $0.02\,\text{eV}\,\text{Å}^{-1}$ for histidine and $0.01502\,\text{eV}\,\text{Å}^{-1}$ for the imidazole ring.

Additionally, we studied the effect of the adsorbed molecules on the electronic transport of graphene, using a non-equilibrium Green's function (NEGF) method, within the density functional theory (DFT), using pseudo-atomic orbitals and pseudo-potentials [21]. We defined a central scattering region sandwiched between a semi-infinite source (left, L_i) and drain (right, R_i) electrode regions. In this case, the studied structures were treated as a one-dimensional infinite cell that consists of the central region denoted by C_0 and the cells denoted by L_i and R_i, where $i = 0, 1, 2, \ldots$ We considered infinite left (L_i) and right (R_i) graphene leads along the a axis under a two-dimensional periodic boundary condition on the bc plane (see Fig. 1). The central region C_0 contained the molecules adsorbed on graphene. The complete modeled device was a supercell of $21.3 \times 12.29 \times 25.00\,\text{Å}^3$, with the two electrodes regions containing 20 carbon atoms each, whereas the central (scattering) region contained 60 carbon atoms belonging to graphene, plus the histidine (or the imidazole ring). The voltage was applied along a axis, and a temperature of 600 K—optimized to obtain a good compromise between accuracy and efficiency in the implementation of the non-equilibrium Green function method [21]—was used in the Fermi–Dirac distribution.

3 Results and discussion

3.1 Adsorption energy and distance

For the study of adsorption, initially we located the molecule at a distance h from graphene, far enough from it ("decoupled"), so a reference energy (E_{ref}) could be determined for the latter calculation of the interaction energy:

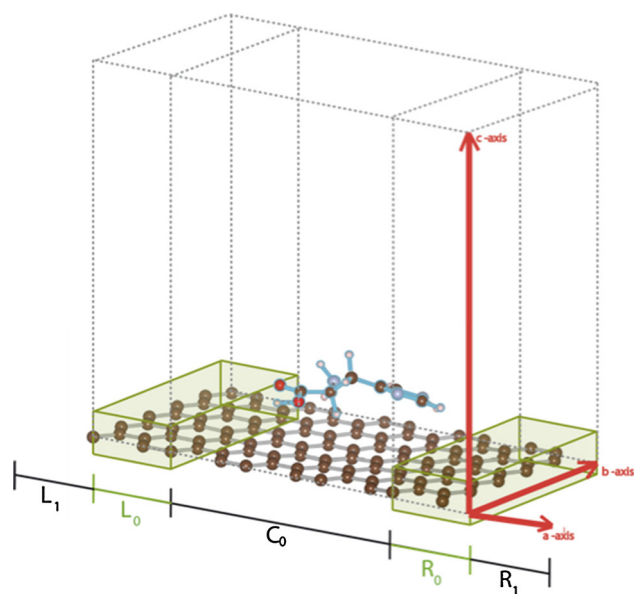$$E_{\text{int}}(h) = E_{\text{tot}}(h) - E_{\text{ref}} \tag{1}$$

Fig. 1 Configuration of the system treated by the NEGF method, with infinite left and right graphene leads along the *a* axis under a two-dimensional periodic boundary condition on the *bc* plane

Fig. 2 Equilibrium geometry for **a** histidine adsorbed and **b** imidazole ring adsorbed

where $E_{ref} = E_{tot}(h = 12.5\,\text{Å})$. In order to determine the adsorption energy and the mean final distance of the biomolecule to the graphene sheet, the molecule (previously relaxed) was placed at several heights. For each height considered, a relaxation for all atoms was performed. Once the adsorbate–substrate system was relaxed, the final average distance (measured from the geometric center of the biomolecule to the graphene sheet) and the interaction energy were obtained. The adsorption energy (E_{ads}) is the lowest interaction energy, while the adsorption distance (d_{ads}) is the one corresponding to the adsorption energy.

The adsorption energy for histidine was greater than for the imidazole ring: $E_{ads\text{-}His} = 1.58\,\text{eV} > E_{ads\text{-}imidazole} = 0.85\,\text{eV}$. The reported values correspond to a strong physisorption of the histidine on graphene. On the other hand, the adsorption distance of the two molecules turned out to be similar: $d_{ads\text{-}His} \approx d_{ads\text{-}imidazole} \approx 2.9\,\text{Å}$. Our results show differences between histidine and the imidazole ring adsorbed on graphene, which is in contrast with what has been assumed in the literature [22]. In Fig. 2, we show the equilibrium configurations, once the molecules were adsorbed: it can be seen that histidine is not oriented parallel to the graphene sheet. This is possibly due to the asymmetry of the molecule: the –COOH and –NH$_2$ groups will tend to interact strongly with the carbon atoms of the graphene sheet, preventing the imidazole ring from being oriented parallel. On the other hand, the adsorbed imidazole ring has a slight angle owing to the interaction between the graphene and a hydrogen atom.
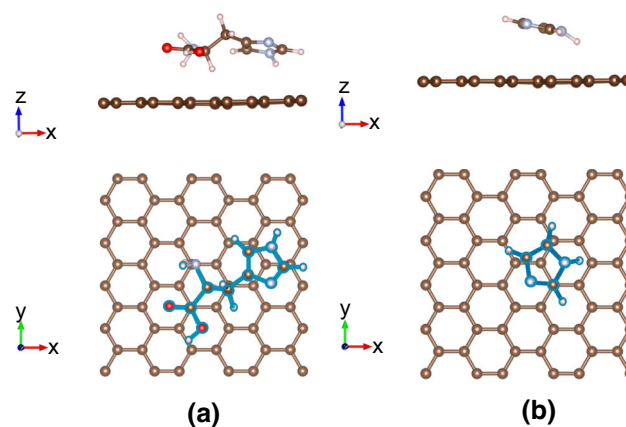
3.2 Charge transfer

The calculated charge transfer from Mulliken population analysis [20] shows a very small charge transfer. We report the existence of a charge transfer from the graphene sheet to the molecule of 0.188 and 0.079 e for histidine and the imidazole ring, respectively. The electronic density redistribution over the graphene sheet induced by the adsorbed histidine was defined as in Ref. [13]:

$$\Delta D = D_{(His+Gra)} - D_{(His)} - D_{(Gra)} \qquad (2)$$

where D denotes the electron charge density. The results are shown in Fig. 3. The violet regions correspond to $\Delta D > 0$, i.e., higher electron density due to adsorption. The gray regions correspond to $\Delta D < 0$, the lower charge density due to adsorption. The gray surfaces are located between the molecule and the graphene sheet; the electrons that participate in π–π interactions cause the charge excess in the molecule (interaction of the *p*-orbitals residing on the imidazole rings and the delocalized *p*-electrons of graphene). For histidine adsorbed, the transferred charge generates a vertical dipole, with the graphene sheet losing charge and the molecule increasing it, as shown in Fig. 3a. For the imidazole ring adsorbed, while still a small charge transfer occurs from the graphene to the ring, the most important effect is a horizontal charge polarization over the graphene sheet forming a longitudinal local dipole, as shown in Fig. 3b. Given that, to the best of our knowledge, there are no experiments reporting on the adsorption of histidine on graphene, these studies should be of interest in the future.

3.3 Electronic transport

Next, we studied the effects of the adsorbed molecules on the electronic transport of the graphene sheet. For the device
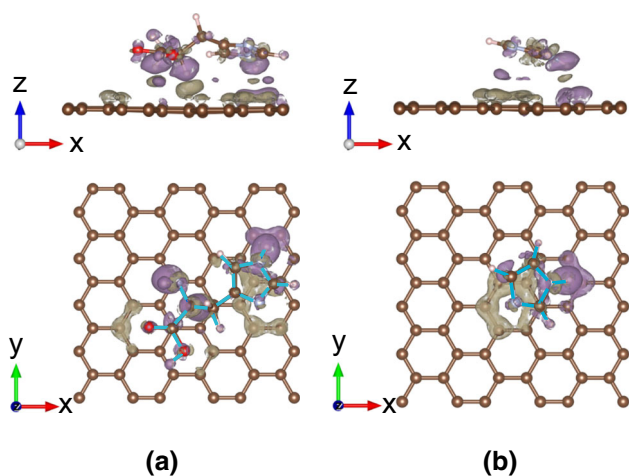
Fig. 3 Charge density. The *violet color* corresponds to regions that accepted electrons ($\Delta D > 0$), while the *gray color* indicates regions that lost electrons ($\Delta D < 0$). **a** Histidine adsorbed on graphene sheet, **b** imidazole ring adsorbed on graphene sheet (Color figure online)

proposed, we introduced bias voltages (V_b) between the two graphene leads in the interval of -2 to 2 V.

The electronic transmission referred to the Fermi energy was obtained according to the following equation:

$$T(E) = \frac{1}{V_c} \int_{BZ} T(E; k) \mathrm{d}k^3 \tag{3}$$

where $T(E; k)$ is the k-resolved transmission, expression within a Green's functions formalism. In Eq. (3) the transmission is evaluated by the Landauer formula for the non-interacting central region C connected with two leads.

In Fig. 4, the transmission for the three systems studied for $V_b = 0$ V is similar. When $V_b = 1$ V, for the graphene sheet alone and the adsorbed imidazole ring, the transmission (1) is similar to each other and (2) higher than that of the adsorbed histidine. For example, an increase in transmission between 0 and 1 eV is clearly observed, a peak above the Fermi level (see arrow).

The device shows sensitivity to histidine for $V_b = 1$ V: a low transmission is presented as compared with that graphene alone (this could be important in relation to the future design of a biosensor. This result agrees with the I–V curve for $V_b = 1$ V: the current for adsorbed histidine is lower in contrast to the other two systems. The current was calculated from the transmission as:

$$I = \frac{e}{h} \int \mathrm{d}E T(E) \Delta f(E) \tag{4}$$

where $\Delta f(E)$ is the difference of Fermi–Dirac distribution functions centered at the electrodes electrochemical potentials.
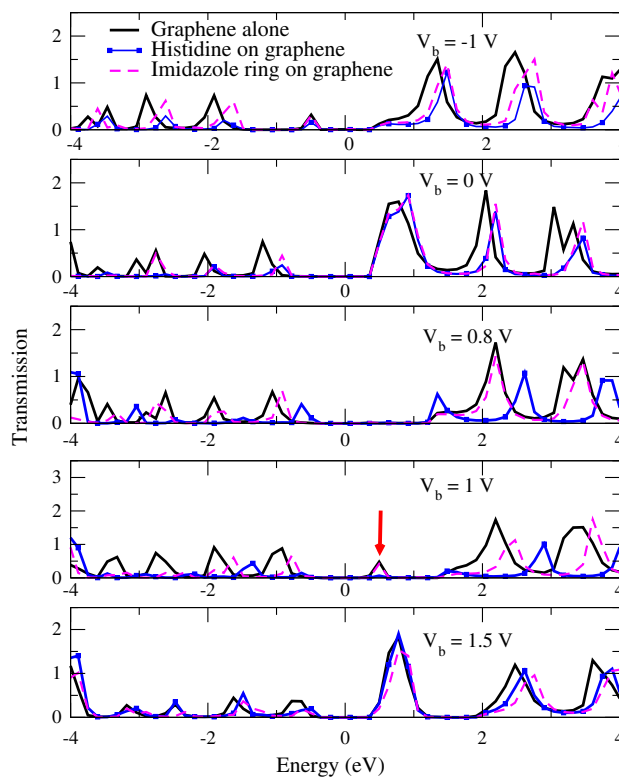

Fig. 4 Transmission for $V_b = -1$, 0, 0.8, 1, 1.5 V for the graphene sheet alone, the histidine adsorbed on graphene, and the imidazole ring adsorbed on graphene. A peak above Fermi energy appears for $V_b = 1$ V (see *arrow*), only for graphene sheet alone and imidazole ring adsorbed; the histidine adsorbed reduces transmission

The current–voltage (I–V) curves are presented in Fig. 5. The I–V curve of the graphene sheet alone exhibits a clear nonlinear behavior, consistent with it being a zero-gap semiconductor. The current is similar for all cases studied when V_b is between -0.4 and 0.4 V. After that, the current becomes dependent on the molecule adsorbed (i.e., the sensor has specificity). Between 0 and 1.5 V the proposed device is relatively insensitive to the imidazole ring, because the current corresponding to the imidazole ring remains close to the current of the graphene sheet alone. However, for $V_b = 2$ V and $V_b = -2$ V the current difference becomes noticeable: 3.71 and 1.75 µA, respectively. In contrast, the currents for the histidine at 1 and -1 V bias voltages were of 1.03 and 1.72 µA, respectively; lower than those of the graphene sheet alone (3.22 and 1.96 µA, respectively). Given that this difference is considerably larger than the pico-ampere electrical sensitivity for graphene-based devices (e.g., graphene field-effect transistor FET biosensor for glucose detection [23], for DNA [24] or two nanotubes connected in parallel for high-current transistors [25]), we conclude that histidine is detectable. The order of magnitude for current reported for some of the available biosensing applications based on graphene FETs is summarized in Table 1. The highest sensitivity to histidine
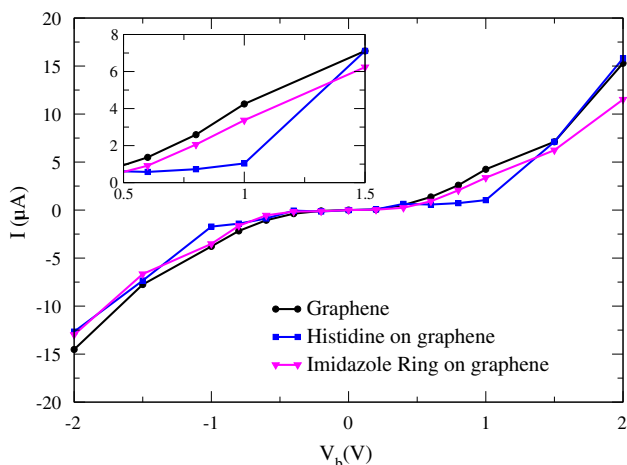
Fig. 5 Current–voltage curve characteristics of graphene sheet alone, graphene with an adsorbed histidine, and graphene with an adsorbed imidazole ring. Bias voltage (V_b) from -2 to 2 V

Table 1 Order of magnitude for current reported on some available biosensing applications based on graphene FETs

Detected biomolecule	Biomolecule	I (μA)	References
Nucleic acids	DNA	4	[26]
	DNA	10	[24]
Protein	Immunoglobulin Ig (G)	0.05	[27]
Bacteria	*E. coli*	5	[11]

happens at $V_b = 1$ V (as the black and blue curves present their maximum difference).

The electronic density redistribution over the graphene sheet induced by the molecules adsorbed for different bias voltages is presented in Fig. 6. We define:

$$\Delta D(V_b) = D_{(V_b)} - D_{(V_b = 0\,\text{V})} \qquad (5)$$

where, $D_{(V_b)}$ is the electronic density for $V_b = -1$, 0.8 and 1 V and $D_{(V_b = 0\,\text{V})}$ is the electronic density for $V_b = 0$ V. When $\Delta D(V_b) > 0$ the electronic density is enhanced by the bias voltages (violet regions). When $\Delta D(V_b) < 0$, the electronic density is reduced by the bias voltages (red regions). For a $V_b = 1$ V, the adsorbed histidine has a lower charge compared to -1 and 0.8 V bias voltages (the same applies to the charge on the graphene sheet center). For all bias voltages, the oxygen atoms of the carboxyl group in the molecule have a higher positive charge density. Still, at some sort the vertical polarization is maintained. On the other hand, when the imidazole ring is adsorbed (i.e., for $V_b = 1$ V, where the current is similar for the imidazole ring adsorbed and the graphene sheet alone): (1) the charge density in the center of the graphene sheet is very low, (2) the charge distribution for
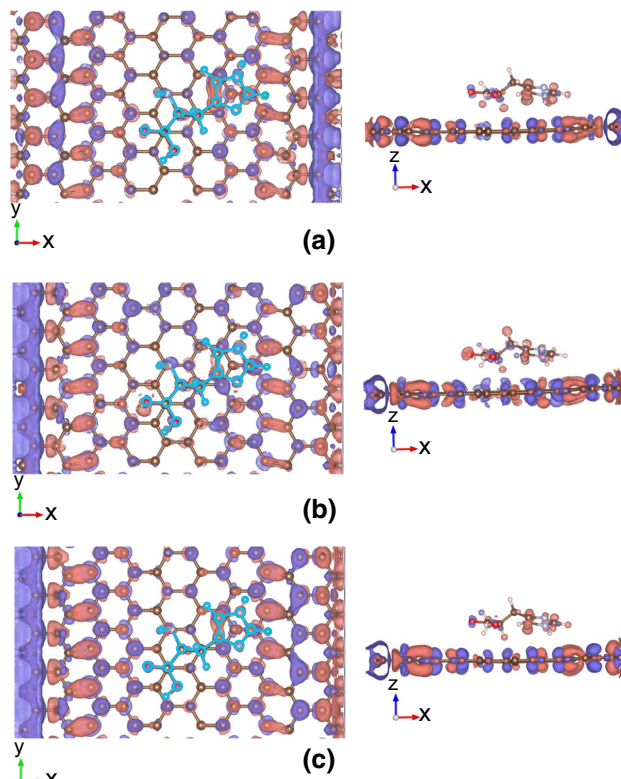

Fig. 6 Charge density of histidine adsorbed on graphene, for different bias voltages V_b (for isosurface level 0.0248 a_0^{-3}, where a_0 is the Bohr radius). *Violet regions* show the electronic density enhanced by the bias voltage. *Red regions* show the electronic density reduced by the bias voltage. **a** $V_b = -1$ V, **b** $V_b = 0.8$ mV and, **c** $V_b = 1$ V (Color figure online)
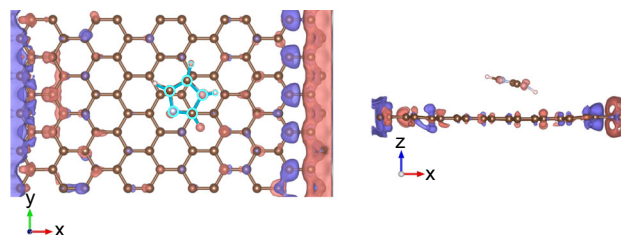

Fig. 7 Charge density of imidazole ring adsorbed on graphene for $V_b = 1$ V (for isosurface level 0.0248 a_0^{-3}, where a_0 is the Bohr radius). *Violet regions* show the electronic density enhanced by the bias voltage. *Red regions* show the electronic density reduced by the bias voltage (Color figure online)

the imidazole ring remains largely unchanged (see Fig. 7 for $V_b = 1$ V).

4 Conclusions

In this work, we modeled a device for the study of the effect of the adsorbed histidine (and imidazole ring) on the electronic transport of a graphene sheet. The transmission and

I–V characteristics differ between histidine and the imidazole ring. We find that adsorption of the imidazole ring alters little the electric current and is undetectable for bias voltages lower than 1.5 V. In contrast, the absorption of histidine is detectable for bias voltages lower than 1.5 V. The theoretical values for the current are the same order of magnitude that the experimental measurements reported for available graphene FET biosensors for biomolecules.

References

1. Geim, A.K., Novoselov, K.S.: The rise of graphene. Nat. Mater. **6**, 183–191 (2007)
2. Ferrari, A.C.: Science and technology roadmap for graphene, related two-dimensional crystals, and hybrid systems. Nanoscale **112**, 1–343 (2014)
3. Baraket, M., Stine, R., Lee, S., Robinson, J., Tamanaha, C.R., Sheehab, P.E., Walton, S.G.: Aminated graphene for DNA attachment produced via plasma functionalization. Appl. Phys. Lett. **100**, 233123 (2012)
4. Huang, B., Li, Z., Liu, Z., Zhou, G., Hao, S., Wu, J., Gu, B.L., Duan, W.: Adsorption of gas molecules on graphene nanoribbons and its implication for nanoscale molecule sensor. J. Phys. Chem. C **112**, 13442–13446 (2008)
5. Georgakilas, V., Otyepka, M., Bourlinos, A.B., Chandra, V., Kim, N., Kemp, K.C., Hobza, P., Zboril, R., Kim, S.: Functionalization of graphene: covalent and non-covalent approaches, derivates and applications. Chem. Rev. **1**, 1–58 (2012)
6. Milowska, K., Majewski, J.: Graphene-based sensors: theoretical study. J. Phys. Chem. C **118**, 17395–17401 (2014)
7. Shao, Y., Wang, J., Wu, H., Liu, J., Aksay, I.A., Lin, Y.: Graphene based electrochemical sensors and biosensors: a review. Electroanalysis **22**, 1027–1036 (2010)
8. Liu, Y., Yu, D., Zeng, C., Miao, Z., Dail, L.: Biocompatible graphene oxide-based glucose biosensors. Langmuir **26**, 6158–6160 (2010)
9. Yang, K., Feng, L., Shi, X., Liu, Z.: Nano-graphene in biomedicine: theranostic applications. Chem. Soc. Rev. **42**, 530–547 (2013)
10. Nelson, T., Zhang, B., Prezhdo, O.: Detection of nucleic acids with graphene nanopores: ab initio characterization of a novel sequencing device. Nano Lett. **10**, 3237–3242 (2010)
11. Huang, Y., Dong, X., Liu, Y., Li, L.J., Chen, P.: Graphene-based biosensors for detection of bacteria and their metabolic activities. J. Mater. Chem. **21**, 12358–12362 (2011)
12. Notley, S.M., Crawford, R., Ivanova, E.P.: Bacterial interaction with graphene particles and surfaces. Nanotechnol. Nanomater. **5**, 99–118 (2013)
13. Song, B., Cuniberti, G., Sanvito, S., Fang, H.: Nucleobase adsorbed at graphene devices: enhance bio-sensorics. Appl. Phys. Lett. **100**, 063101 (2012)
14. Lee, E.C.: Effects of DNA nucleotide adsorption on the conductance of graphene nanoribbons from first principles. Appl. Phys. Lett. **100**, 153117 (2012)
15. Zhang, Y.H., Zhou, K.G., Xie, K.F., Zeng, J., Zhang, H., Peng, Y.: Tuning the electronic structure and transport properties of graphene by noncovalent functionalization: effects of organic donor, acceptor and metal atoms. Nanotechnology **21**, 065201 (2010)
16. Rodríguez, S., Makinistian, L., Albanesi, E.: Theoretical study of the adsorption of histidine amino acid on graphene. J. Phys. Conf. Ser. **705**, 012012 (2016)
17. Ortmann, F., Schmidt, W., Bechstedt, F.: Attracted by long-range electron correlation: adenine on graphite. Phys. Rev. Lett. **95**, 186101 (2005)
18. Lee, J., Choi, Y., Kim, H., Scheicher, R., Cho, J.: Physisorption of DNA nucleobases on h-BN and graphene: vdW-corrected DFT calculations. J. Phys. Chem. C **117**, 13435–13441 (2013)
19. Grimme, S.: Semiempirical GGA-type density functional constructed with a long-range dispersion correction. J. Comput. Chem. **27**, 1787 (2006)
20. Ozaki, T.: Numerical atomic basis orbitals from H to Kr. Phys. Rev. B. **67**, 155108 (2003)
21. Ozaki, T., Nishio, K., Kino, H.: Efficient implementation of the nonequilibrium Green function method for electronic transport. Phys. Rev. B **81**, 035116 (2010)
22. Rajesh, C., Majumder, C., Mizuseki, H., Kawazoe, Y.: A theoretical study on the interaction of aromatic amino acids with graphene and single walled carbon nanotube. J. Chem. Phys. **130**, 124911 (2009)
23. You, X., Pak, J.J.: Graphene-based field effect transistor enzymatic glucose biosensor using silk protein for enzyme immobilization and device substrate. Sens. Actuators B **202**, 1357–1365 (2014)
24. Cai, B., Wang, S., Huang, L., Ning, Y., Zhang, Z., Zhang, G.J.: Ultrasensitive label-free detection of PNA-DNA hybridization by reduced graphene oxide field-effect transistor biosensor. ACS Nano **8**, 2632–2638 (2014)
25. Zhang, T., Nix, M.B., Yoo, B.Y., Deshusses, M.A., Myung, N.V.: Electrochemically functionalized single-walled carbon nanotube gas sensor. Electroanalysis **12**, 1153–1158 (2006)
26. Dong, X., Fu, D., Xu, Y., Wei, J., Shi, Y., Chen, P., Li, J.: Label-free electronic detection of DNA using simple double-walled carbon nanotube resistors. J. Phys. Chem. **112**, 9891–9895 (2008)
27. Mao, S., Lu, G., Yu, K., Bo, Z., Chen, J.: Specific protein detection using thermally reduced graphene oxide sheet decorated with gold nanoparticle-antibody conjugates. Adv. Mater. **22**, 3521–3526 (2010)